FOUR-COLOR LASER IRRADIATION SYSTEM FOR LASER–PLASMA INTERACTION EXPERIMENTS

D. M. Pennington
T. L. Weiland
M. A. Henesian
D. Eimerl
R. B. Wilcox

Introduction

Since 1986, optical smoothing of the laser irradiance on targets for Inertial Confinement Fusion (ICF) has gained increasing attention.[1–5] Optical smoothing can significantly reduce wavefront aberrations that produce nonuniformities in the energy distribution of the focal spot. Hot spots in the laser irradiance can induce local self focusing of the light, producing filamentation of the plasma. Filamentation can have detrimental consequences on the hydrodynamics of an ICF plasma, and can affect the growth of parametric instabilities, as well as add to the complexity of the study of such instabilities as stimulated Brillouin scattering (SBS) and stimulated Raman scattering (SRS).[6–10] As experiments approach and exceed breakeven (i.e., where driver energy = fusion yield), the likelihood of significant excitation of these processes increases. As a result, we are including a scheme for implementing optical-beam smoothing for target experiments in the baseline design for the proposed next-generation ICF facility—the National Ignition Facility (NIF).[11]

To verify the efficacy of this design for the suppression of parametric instabilities in NIF-like indirect-drive targets, we successfully modified a Nova beamline to simulate the proposed NIF conditions. In this article, we discuss the laser science[12] associated with a four-color target campaign on Nova to test the effect of *f*-number (ratio of focal length to beam diameter) and temporal smoothing on the scaling of SBS with a four-segment interaction beam using NIF-like parameters. The results of the target series associated with the four-color configuration are discussed in "Laser–Plasma Interactions in Large Gas-Filled Hohlraums," p. 97 of this *Quarterly* and elsewhere.[13–15]

The NIF[11] design has four beamlets per beamline, which overlap to form an effective $f/8$ beam focus. Each beamlet is smoothed by a random phase plate (RPP). RPPs consist of many randomly distributed on/off phase elements deposited on a fused-silica substrate.[16,17] The focal-plane intensity distribution resulting from focusing light through a bilevel RPP consists of an overall envelope, modulated by fine-scale spatial structure within that envelope. The envelope is produced by diffraction from a single-phase element, and the fine-scale structure, or speckle, is due to the superposition of the diffraction patterns from each of the phase elements. The speckle size corresponds to the diffraction limit of the full-aperture beam incident on the RPP. Because speckle size increases with *f*-number, an $f/8$ beam should filament more than the $f/4.3$ beams on Nova.[18,19] Simulations indicate that SBS reflectivity increases due to filamentation, with a total gain greater than calculated for a uniform laser intensity. SBS reflectivities >10% may unacceptably degrade target performance by disrupting symmetry or reducing the energy available for radiation heating. The introduction of temporal and spatial incoherence over the face of the beam using techniques such as smoothing by spectral dispersion (SSD)[1] or induced spatial incoherence (ISI)[5] reduce the rms-intensity variations in the laser irradiance when averaged over a finite time interval, providing temporal smoothing. Temporal smoothing makes filamentation less likely because the filament must form before the hot spot moves to a different location.

Figure 1 is a schematic of the SSD technique. Broadband light, produced in this case by electro-optic phase modulation (FM), is spectrally dispersed by a grating, and then amplified, frequency converted, and focused through an RPP on to a target. Each distinct frequency component produces a speckle pattern, resulting in a superposition of many speckle patterns. Since each frequency propagates at a different angle through the phase plate, the speckle patterns spatially shift as a function of frequency. As the frequencies change throughout the length of the pulse, the rapidly

UCRL-LR-105821-95-2

fluctuating interference of the displaced speckle fields for the different spectral components causes the irradiance to appear smooth on a time-averaged basis. The most effective beam smoothing is obtained when the speckle field for each spectral component is spatially shifted at the target plane by at least one-half speckle diameter, $d_{1/2} = 1.22\lambda f/D$, where D is the beam diameter on the phase plate, λ is the third harmonic (3ω, 351 nm) wavelength, and f is the focal length of the lens.[4] This level is achieved when the 3ω dispersion at the output aperture is fixed at $d\theta/d\nu = d_{1/2}/f\cdot\delta\nu$ in rad/Hz, for a specified spacing between spectral components, $\delta\nu$, and speckle size, $d_{1/2}$.

The time-integrated smoothness, σ/I, is defined as the spatial rms-intensity variance normalized to the average at the target plane. The smoothness is equal to $1/\sqrt{N}$, where N is the number of decorrelated speckle fields superimposed at each point on the target. The effective time-integrated smoothing level for spectrally dispersed beams can be approximated by

$$\sigma/I = \sqrt{\tau\,\delta\nu} = \left[\frac{1.22\lambda\tau}{D}\left(\frac{d\theta}{d\nu}\right)^{-1}\right]^{\frac{1}{2}} \qquad (1)$$

where $\delta\nu$ is the effective separation between independent spectral components in Hz, τ is the coherence time in seconds (inverse of the frequency-converted bandwidth), and $d\theta/d\nu$ is the spectral dispersion at 3ω in rad/Hz. For optimal dispersion, N is the total number of spectral components in the beam and $\delta\nu$ is the modulation frequency of the electro-optic phase modulator. Instantaneously, $\sigma/I \cong 1$ due to basic Rayleigh speckle statistics, but this value decreases rapidly as the irradiance variations are averaged over time. The initial smoothing occurs on a time scale proportional to $1/\tau$, reaching the asymptotic level given by Eq. (1) in a time determined by $1/\delta\nu$. The initial onset of smoothing is delayed due to the spatially varying time delay across the beam imposed by the grating (i.e., a delay of λ/c per illuminated grating line). This time delay δt is proportional to $1/\delta\nu$, and therefore N is proportional to $\delta t/\tau$.

In the case of m beamlines, each with a different central frequency and n decorrelated FM components per beamline, $\sigma/I = 1/\sqrt{N}$, where $N = nm = \Delta\nu/\delta\nu$. The value of D in Eq. (1) becomes the individual beamlet diameter, and the coherence time τ is proportional to $1/\Delta\nu$, where $\Delta\nu$ is the total bandwidth of the four FM-modulated central frequencies. With a four-color segmented beam, as used in the current Nova experiments, the superposition of the four narrowband speckle fields should produce a smoothing level of 50% ($\sigma/I = 0.5$) at the target plane. Since all four colors are present simultaneously throughout the pulse, the asymptotic level is achieved within a few picoseconds. The smoothing rate is proportional to the number of beamlines and is unaffected by the grating time delay, δt. The resulting pattern fluctuates with a periodicity determined by the narrowest frequency separation. The addition of FM bandwidth to the four-color beam allows additional temporal smoothing by creating many additional decorrelated speckle fields. This smoothes very rapidly due to the wide overall bandwidth. The rate of four-color beam smoothing with FM bandwidth and spectral dispersion is four times faster than one-color FM smoothing, assuming the same bandwidth per beamline, reaching a 50% lower σ/I at the same f-number per beamlet.

One of the primary limitations on previously used beam-smoothing techniques is the reduced frequency conversion efficiency to the third harmonic due to bandwidth.[20] High-efficiency frequency tripling can be achieved only over a narrow spread in wavelength for a given crystal phase matching condition; thus to remain within 10% of the maximum conversion efficiency, the input bandwidth should be limited to ~0.2 nm, or ~60 GHz. However, while beam smoothness is strongly dependent on both the amount of dispersion and spectral bandwidth used, the larger the bandwidth (i.e., the shorter the coherence time), the more rapidly the structure changes, and the more rapidly the time-averaged intensity smoothes.

The NIF design can simultaneously achieve high third-harmonic conversion efficiency with broad

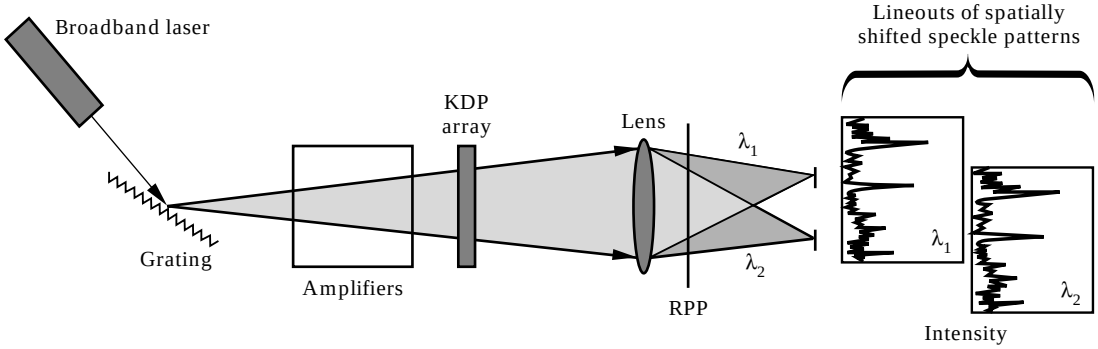

FIGURE 1. Schematic illustration of the smoothing by spectral dispersion (SSD) technique.
(70-00-0395-0824pb01)

bandwidth for rapid smoothing. The NIF is proposed to have four beamlets focused to a single spot per beamline, each with a different frequency and separated by 1 nm.[11] Each individual beamlet will have a bandwidth of only 0.25 nm, allowing high-efficiency frequency tripling. The superposition of four beamlets with different frequencies will produce the wide overall-spectral width required for good temporal smoothing.

To simulate this configuration, a Nova beam was modified to have an $f/8$ geometry, with a segmented four-quadrant beam. We developed a multifrequency bandwidth source that is spatially separated into four quadrants, each containing a different central frequency separated by up to 0.88 nm. Each quadrant is independently converted to the third harmonic in a four-segment Type I/Type II potassium dihydrogen phosphate (KDP) crystal array with independent phase matching in each quadrant for efficient frequency conversion of the four frequencies. In addition, a limited amount of bandwidth (~0.2 nm) can be added to each frequency component to more closely approach a continuous broadband spectrum. We compared the results obtained with this method with those previously obtained on Nova with a continuous bandwidth source and a single-frequency conversion array.[20] Using this method, we obtained a factor of four increase in 3ω output energy with comparable overall bandwidth.

Four-Color Implementation on Nova

Significant modifications to the oscillators, mid-chain optics, SSD table, frequency-conversion arrays, laser diagnostics, target diagnostics, and final focus lens allowed implementation of four-color capability on Nova, as shown in Fig. 2. To perform target experiments, the four-color input spectrum must be stable to ±10% in energy, with frequency jitter <0.0019% and be reproducible from shot to shot. Energy balance between the four quadrants must be better than ±10% at 1ω and ±20% at 3ω. The composite beam is required to have $>2\times10^{15}\ \mathrm{W/cm^2}$ at the third harmonic in a 500-μm-diam focal spot. This section describes the modifications

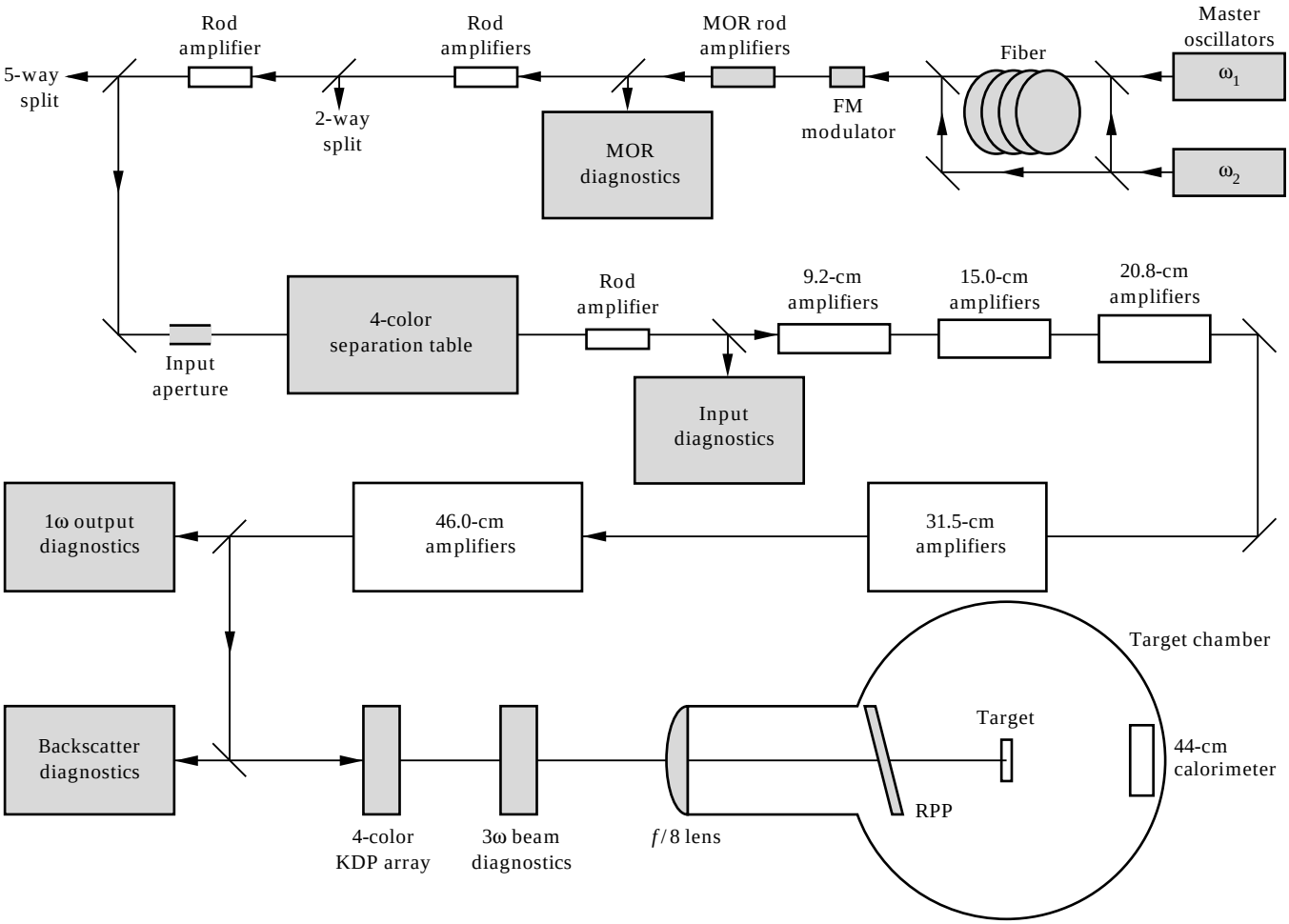

FIGURE 2. Layout of Nova's four-color system. Areas modified to accommodate the four-color system are shaded. (70-00-0395-0792pb01)

required to meet these conditions and the overall laser performance of the four-color system.

Four-Color Bandwidth Source

Four-color target experiments required the development of a four-color laser source with a bandwidth capability similar to that planned for the NIF. The technique chosen to provide the four discrete frequencies is based on the nonlinear mixing of two frequencies in an optical fiber. Two photons at the pump frequencies are annihilated to create two photons at frequencies shifted toward the blue and red sides.[21,22] These newly created spectral components result in self-phase modulation (SPM)-induced broadening of the pulse. The phase shift incurred by propagation through the fiber is proportional to the fiber length L and the pulse intensity I, and the number of sidebands generated is linearly proportional to this phase shift. The number of lines generated is controlled by changing the pump intensity into the fiber, while the separation between frequencies is varied by tuning the frequencies of the oscillators. This technique produces a broad comb of discrete single-mode frequencies (up to ~40 lines), which can be spectrally separated to provide a tunable single-frequency source.

We produce the two-frequency input to the fiber by etalon-tuning two single longitudinal mode, Q-switched Nd-doped yttrium lithium fluoride (Nd:YLF) oscillators[23] to 1053.23 nm and 1052.79 nm, respectively. The measured frequency variation of each oscillator is <0.0016%. The output beams are temporally and spatially overlapped, and shortened to a 15-ns nominally square pulse and coupled into a single-mode polarization preserving fiber. The spectrally integrated beam energy is recorded at the input and output of the fiber. The time-integrated and time-resolved output spectra and spectrally integrated pulse shape are also recorded.

Time-integrated spectral measurements, like the example shown in Fig. 3(a), indicate that the energy content of the central spectral lines remains constant to within ±10% as the input energy increases and the spec-

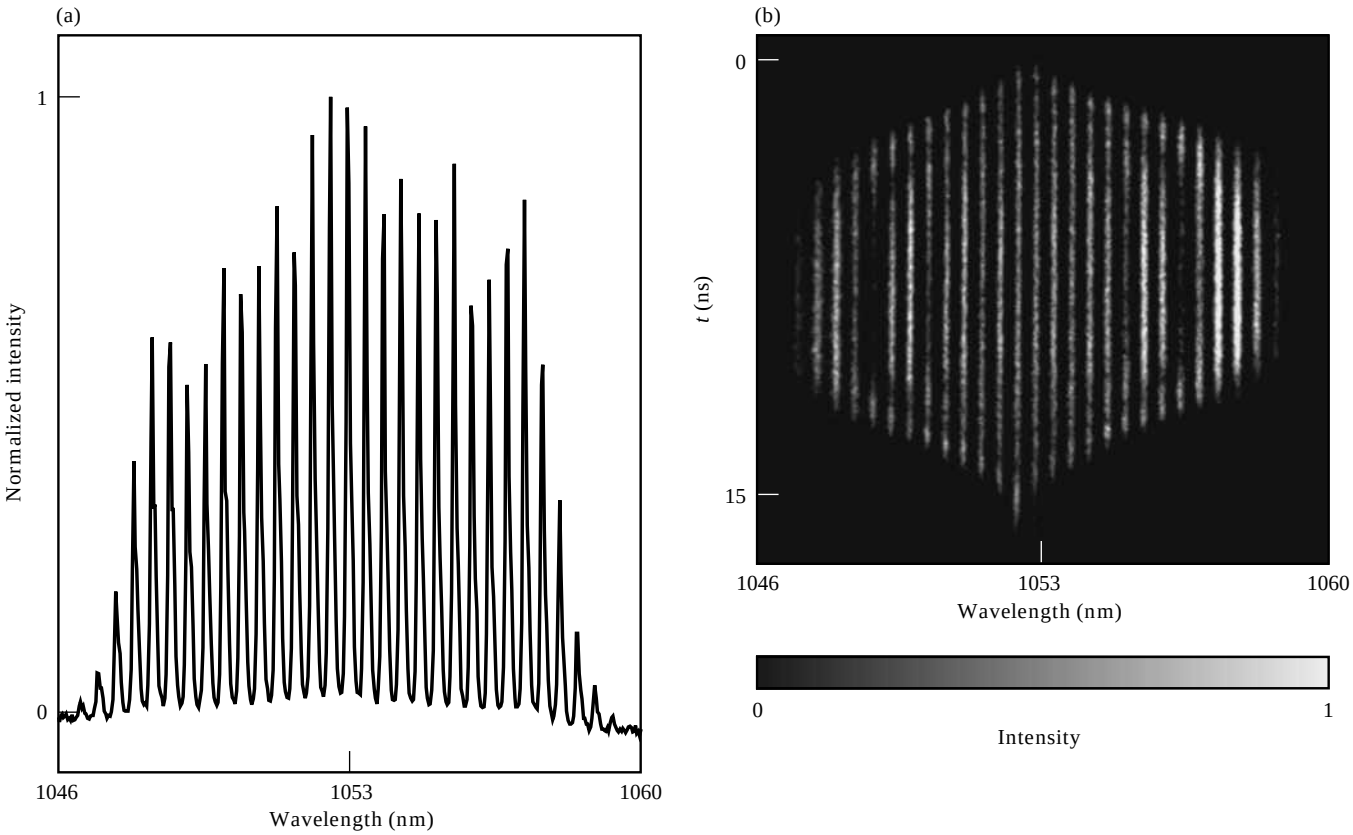

FIGURE 3. Multifrequency spectrum generated by self-phase modulation of two frequencies separated by 0.44 nm in an optical fiber. (a) Shows a representative time-integrated spectrum for an intensity-length product, IL = 1.2 TW/cm. (b) Shows the temporal evolution of the same spectrum. The number of spectral lines increases and decreases linearly with the 4-ns rise and fall of the pulse. (70-00-0395-0793pb02)

trum broadens. The amplitude between lines varies <±10%, while the output energy of the integrated spectrum varies <±3% from shot to shot. A maximum spectral width of 14-nm full-width at half maximum (FWHM) is obtained by this technique. The temporal buildup of the SPM spectrum, shown in Fig. 3(b), reflects the change in pulse intensity caused by the 4-ns rise and fall time of the input pulse. The central 3–5-ns section of the 15-ns pulse is nominally flat in time across the generated spectrum. A temporally uniform 1-ns slice is selected from the center of that section by the main pulse shaping system in the Master Oscillator Room (MOR), then shaped to precompensate for square-pulse distortion later in the laser chain.[24,25] The time-resolved spectra shown in Fig. 4 demonstrate that each spectral component is stable on the time scale required for four-color experiments for low- and high-energy input to the fiber.

To produce the main pulse for the other nine Nova beams, we split off a percentage of the energy in one of the frequencies before it enters the fiber, as shown in Fig. 2. The split-off pulse is then re-injected into the main beam path before it enters the temporal pulse shaping system. Following spectral and temporal shaping, the beam propagates through a double-pass electro-optic phase modulator, which allows the addition of 0.2 nm of FM bandwidth to each frequency component to provide SSD. The time-resolved spectrum of the FM-modulated pulse is shown in Fig. 4(c). Since both the multifrequency and single-frequency beams share this beam path, FM bandwidth is present on all 10 Nova beamlines when the modulator is active.

Grating Separator

The multifrequency beam from the MOR is amplified in the preamplifier section of Nova, where its energy increases to several Joules before being routed to the appropriate beamline. The time-multiplexed multifrequency and single-frequency beams are separated into different beamlines by a Pockels cell / polarizer combination in the preamplifier section. The multifrequency pulse is directed to beamline 7 (BL7), which contains the wavelength separation optics, while the single-frequency pulse is sent to the other nine beamlines via beam splitting and delay optics. The four-color separation optics in BL7 introduce sufficient delay, relative to the other arms, to allow all pulses to arrive simultaneously at the target.

We modified the existing SSD table[2] in BL7 to accommodate the four-color separation optics. These optics, shown schematically in Fig. 5, convert the single multifrequency beam into a four-quadrant beam with one frequency per quadrant. The system is equivalent to four monochrometers sharing a common output slit; as a result, the four output beams are coincident and parallel. This "multichrometer" consists of a four-segment grating array followed by a 1:1 relay with the slit at the focal plane. The image of the grating array is relayed to the output plane where the wavelength of

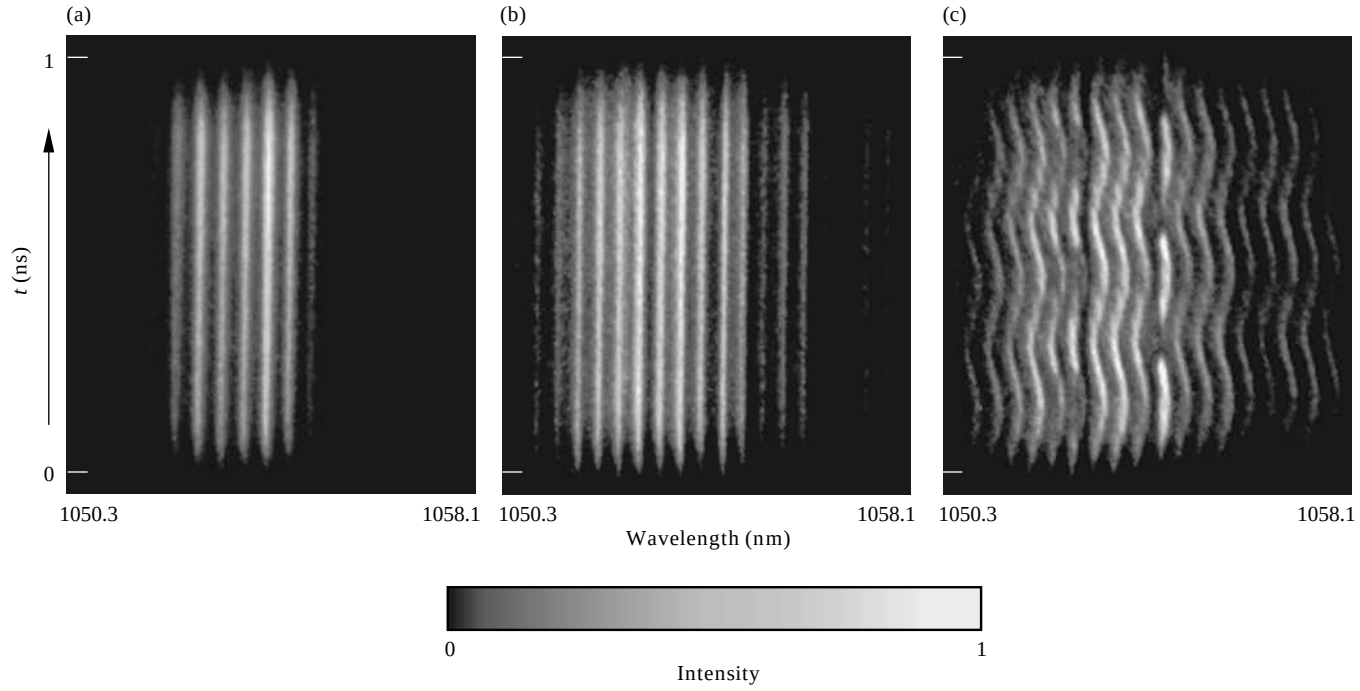

FIGURE 4. The time-resolved spectra of the amplified 1-ns sliced pulse demonstrate that each component of the multifrequency spectrum is stable on the time scale required for four-color experiments. The separation between each color is 0.44 nm. (a) Low-energy input to the fiber, *IL* = 0.2 TW / cm. (b) High-energy input to the fiber, *IL* = 1.3 TW / cm. (c) High-energy input into the fiber with 0.2 nm of FM bandwidth per component, *IL* = 1.3 TW / cm. (70-00-0594-2299pb01)

each segment is selected by independently angle tuning each grating. The unwanted frequencies in each segment are blocked by the slit. A charge-coupled device (CCD) camera imaging the slit monitors the unselected frequency components, allowing alignment of the grating components before each shot. A spectrometer after the slit provides a record of the four-color output spectrum.

The gratings separate each of the four main frequency components with up to 0.3 nm of FM bandwidth per frequency, by more than the focal spot size, allowing passage through the slit without interference from adjacent frequency-modulated bandwidth components. In addition, sufficient dispersion is used to separate each frequency-modulated bandwidth component at the target by at least one-half speckle diameter to achieve optimal beam smoothing. We chose 1800 grooves / mm gratings with a dispersion of 5.64×10^{-3} rad / nm at 1053 nm to meet these constraints. The gratings used in the array were fabricated in-house to obtain the highest possible diffraction efficiency and damage threshold.[26] To reduce the temporal delay of the pulse front across the beam, the gratings are arranged in a "V" configuration. This reduces the temporal skew from 600 to 300 ps, producing a chevron–shaped temporal distortion across the face of the beam, symmetric about the horizontal midline. The non-Littrow grating configuration produces a geometric distortion that is corrected with a four-quadrant heart-shaped apodizer, as shown schematically in Fig. 5. This preforms the beam into a heart-shaped design before the grating array, which then diffracts into a circular beam.

To compensate for unequal SPM sideband amplitudes, the line shape of the amplifier gain, and other spectral inhomogeneities, we independently adjust the energy in each segment to achieve an equal distribution of energy at the target. To balance the quadrant energies, a four-quadrant array of absorbing filters, adjustable in 5% increments, is placed before the grating. Rod shots, in which only the preamplifier section fires, are used to balance the energies between the quadrants. Using this method, better than ±6% energy balance at 1ω and ±17% at 3ω is routinely achieved.

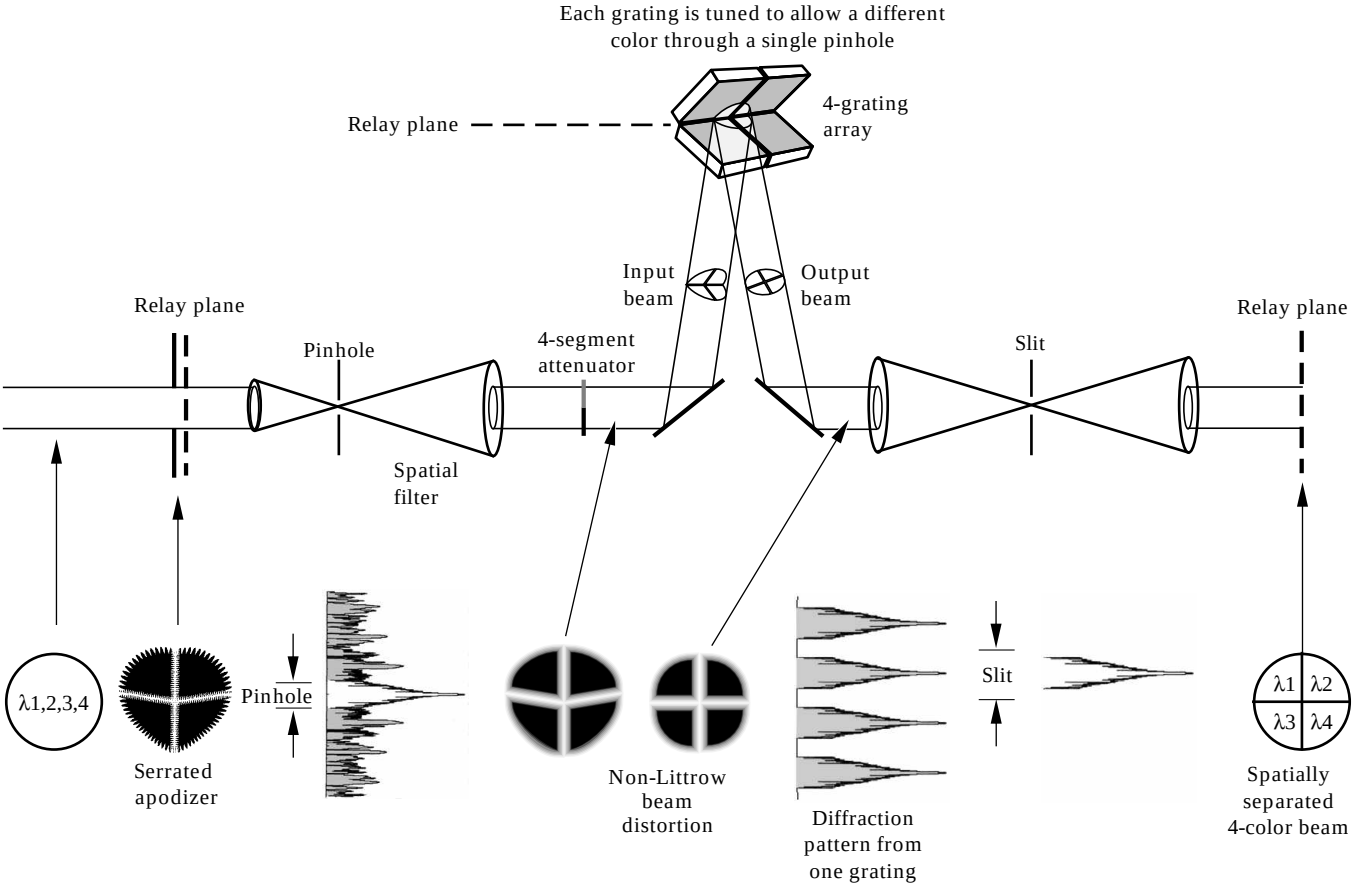

FIGURE 5. Schematic of the special optics installed in the four-color beamline to convert the single multifrequency beam into a four-quadrant beam with one frequency per quadrant. In the output plane, the wavelength of each segment is selected by independently angle-tuning each grating. The unwanted frequencies are blocked by a slit at the focal plane. The beam shape is preformed into a heart-shaped design before the grating array, which diffracts into a circular beam due to the grating configuration. (70-50-0993-3246pb01)

Frequency Converter

The full-aperture 2 × 2 frequency conversion array, shown in Fig. 6, converts the four-color beam to the third harmonic. Each quadrant contains a 12-mm-thick Type I doubler and a 10-mm-thick Type II tripler, using 27-cm Nova KDP crystals. We use the Type I/Type II frequency tripling scheme because of increased performance previously demonstrated on Nova,[20,27] and its adaptability to angle tuning. The four crystal segments are mechanically offset in angle and independently tunable, to allow placement of any of the four wavelengths in each quadrant. The array allows independent tuning of all eight crystals, although the bandwidth of the doublers is sufficient to accommodate the frequency span of the four colors with a single angular orientation. Although the area provided by the four 27-cm crystals is smaller than the full Nova aperture (~80%), the expected energy on target is sufficient for four-color target experiments. We chose the crystal separation to maximize the beam area (~2600 cm^2), compatible with the beam apodization on the grating separation table. Once installed and aligned, a rocking curve was performed to tune the array for maximum performance. This four-color array design achieves up to 65% 3ω conversion efficiency, providing up to 2.3 kJ on target.

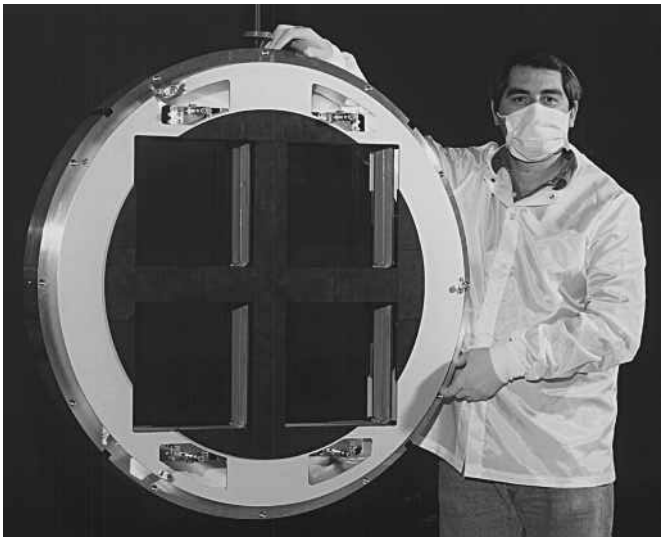

FIGURE 6. Photograph of the Type I/Type II four-color frequency conversion array. (70-10-0494-2032pb01)

Four-Color System Performance

1ω Propagation Experiments

We performed a series of 1ω propagation tests to assess various issues associated with the propagation of a multifrequency beam through the Nova preamplifier section. The energy and near-field image of the unsegmented multifrequency beam are recorded midway through the Nova preamplifier section. The characteristics of the 1ω segmented four-color beam are recorded in the input sensor immediately following separation, and again in the output sensor package before conversion to the third harmonic. The output sensor diagnostics include near-field photography of the spatially separated four-color beam, measurement of the integrated beam energy via calorimetry and diode measurements, and measurement of the integrated pulse shape of the full beam. The energy in each frequency is determined by integrating the fluence in each quadrant of the output sensor near-field camera. A 1-m spectrometer provides a time-integrated spectrum of the full beam. In addition, an array of four photodiodes records the pulse shape of the individual frequencies.

We observe substantial spectral gain narrowing of the SPM spectrum in the Nova chain. Amplification (gain ~ 10^{21}) reduces the unamplified SPM spectrum shown in Fig. 3(a) from ~9.8 nm FWHM to the ~2.1 nm FWHM spectrum shown in Fig. 7(a). This results from spectral gain narrowing produced by the 2.15-nm

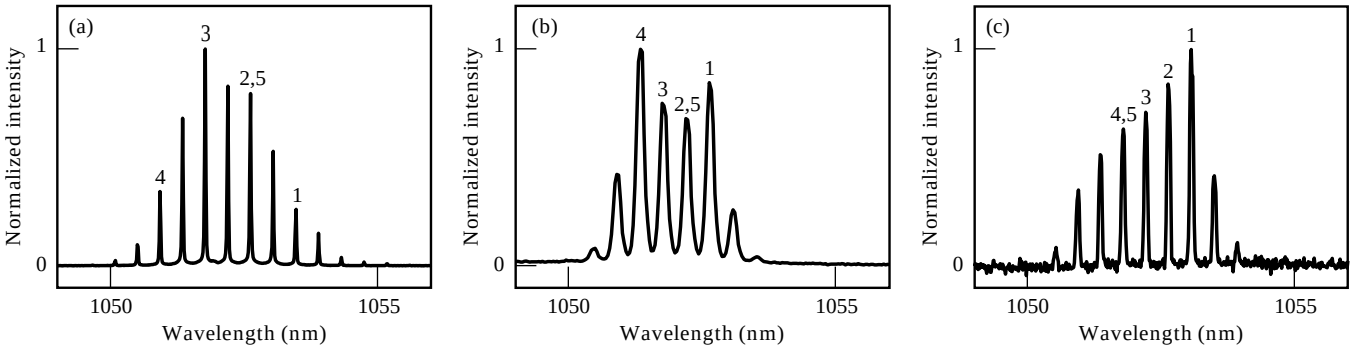

FIGURE 7. (a) Significant gain narrowing of the input spectrum occurs after full amplification in the Nova chain (gain ~ 10^{21}). A frequency spacing of 0.88 nm can be obtained with this spectrum by selecting alternate lines. (b) The central four lines of a low-power SPM spectrum produce a 0.44-nm separation for the first set of four-color target experiments. (c) A series of lines offset from the center of the spectrum are selected for the second four-color target series. The four colors selected by the grating array are indicated by 1, 2, 3, and 4, while 5 is the heater beam frequency. (70-00-0395-0794pb02)

FWHM fluorescence line width of Nd:glass[28] and bandwidth limiting components in the laser chain. As the extraction frequency moves off the peak of the laser glass fluorescence spectrum, the gain coefficient decreases. Thus, to maintain a constant output fluence from the amplifier chain, the input energy must increase to compensate for the reduction in gain off the peak. Experimental measurements show that although the gain and saturation fluence differ for each wavelength as expected, the differences in square pulse distortion are minimal. We performed small-signal gain measurements for the multifrequency spectrum by propagating low-power shots through the laser chain without firing the disk amplifier section. These measurements indicate that the maximum bandwidth that can be supported by the Nova chain is ~3 nm. At maximum bandwidth, it is necessary to keep the energy in the preamplifier section below the fluence threshold for self-focusing and other nonlinear interactions.

For the first four-color target series, we chose a 0.44-nm separation between the four selected frequencies. The intensity propagated through the optical fiber was reduced to allow the generation of only six lines, as shown in Fig. 7(b). The four lines selected on the grating table are centered on the peak of the Nd:glass gain curve to maximize the gain in the amplifier chain, producing 6 kJ at 1ω in 1 ns. Figure 7(c) shows the 8-line spectrum propagated to the grating array for subsequent target experiments. For these experiments, the four-color gratings were tuned to select four colors shifted off the peak of the gain curve. Four colors with a maximum separation of 0.88 nm can be obtained by selecting alternate lines in the SPM spectrum shown in Fig. 7(a), with sufficient 3ω energy to perform target experiments simulating the NIF frequency separation.

Figure 8 compares the pulse shape of each frequency at the source and the output of the laser chain for a 0.44-nm separation between the four colors. The pulse shapes of each frequency at the source, shown in Fig. 8(a), are comparable to within the diagnostic background noise. In Fig. 8(b), the four-quadrant output-diode traces show that three of the pulses lie on top of each other, while the fourth shows a slight difference in contrast ratio, consistent with the higher output fluence in this quadrant. At this fluence and line separation, it is possible to balance the 1ω energy between the four quadrants to better than ±6%, with temporally smooth pulses to within the diagnostic resolution. Figure 9 shows a representative near-field image of the 1ω beam taken with the output sensor diagnostic CCD camera.

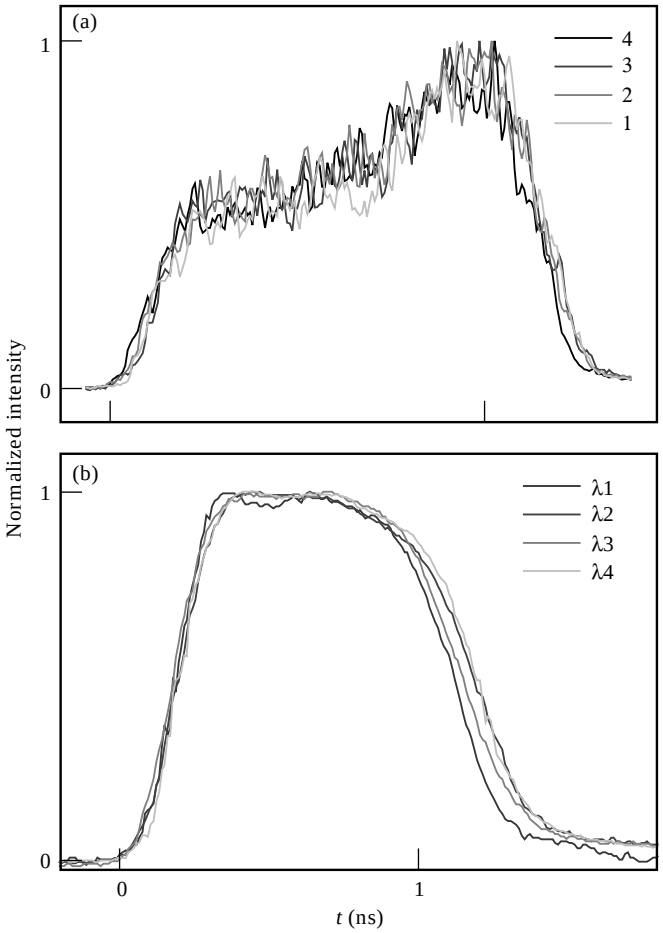

FIGURE 8. Comparison of the temporal pulse shape for each of the four colors (a) at the source and (b) at the output of the laser chain for a 0.44-nm separation. (70-00-0395-0795pb01)

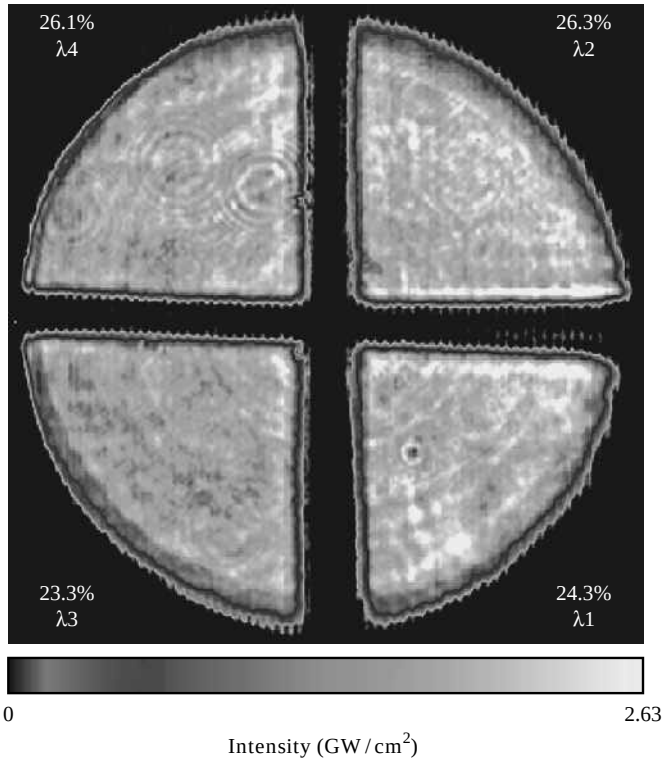

FIGURE 9. Representative near-field image of the 1ω beam taken with the output sensor diagnostic CCD camera. The 1ω energy in each of the four quadrants is balanced to better than ± 6%. (70-00-0495-0924pb01)

Four-Color Beam Smoothing

The two-beam laser diagnostic station (TBLDS)[29] was used to characterize the beam smoothing properties of the four-color irradiance. We used a 3.3-mm-diam, square element phase plate with the standard Nova $f/4.3$ focal geometry to produce approximately the same size focal spot (550 μm) as the $f/8$ geometry in the 10-beam chamber. The near-field, far-field, and expanded far-field images; temporal profile, energy, and spectra were recorded in the TBLDS following frequency conversion to the third harmonic. Figure 10 shows the effect of beam smoothing at 3ω in the equivalent target plane images for (a) an unsmoothed Nova beam; (b) a single-frequency beam with an RPP; (c) a four-color beam with 0.44 nm, or 122 GHz, separation between colors at 1ω and an RPP; and (d) a four-color beam with 0.2 nm or 5.4 GHz of FM bandwidth per component at 1ω and an RPP. All four images have equivalent magnification. The nonuniformities in the unsmoothed irradiance shown in Fig. 10(a) demonstrate the need for beam smoothing. The far-field image of a single-frequency beam with the RPP in Fig. 10(b) shows that the intensity structure is broken up into a homogeneous well-controlled speckle pattern. This pattern remains static throughout the pulse length. The normalized rms variance of the focal irradiance, σ/I, is ~0.79 for this image. This is less than the theoretical predicted value of one for a single speckle pattern, but consistent with previous measurements on Nova and elsewhere.[20,30] This may be an indication that some polarization smoothing is occurring due to birefringence in the focus lenses. In Fig. 10(c), the pattern produced by the four-color beam shows the smoothing obtained by superposition of four independent speckle patterns, with the significant residual speckle structure expected from the limited number of static patterns. The four-color beam produces a time-integrated smoothing level of $\sigma/I \sim 0.25$, in contrast to the theoretically predicted value of $\sigma/I = 0.50$. The reduced σ/I may be associated with the effects seen in Fig. 10(b). Also note that the intensity-length product for these experiments exceeds the threshold for stimulated rotational Raman scattering in air by ~25%,[31,32] as observed experimentally. The chromatic dispersion of this additional bandwidth by the additional optics used to direct the beam to the TBLDS may also contribute slightly to the lower σ/I measured on this shot. Figure 10(d) clearly shows that SSD with four colors and FM bandwidth produces a much smoother focal spot than the previous three images. Discrete speckles are no longer observable and the irradiance is smooth and uniform. The vertical streaks in the image are formed by the one-dimensional nature of the dispersion. This image has a $\sigma/I \sim 0.16$. This is less smooth than theoretically predicted, but is consistent with previous measurements of smoothing with FM bandwidth on Nova.[20]

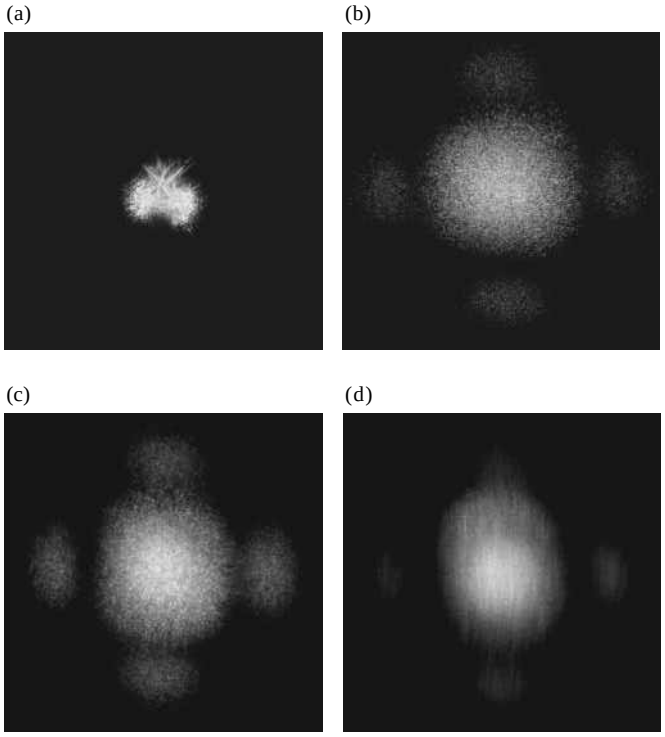

FIGURE 10. (a) Nonuniformities in the equivalent target plane image of the 3ω beam at best focus demonstrate the need for beam smoothing. The effect of beam smoothing at 3ω can be seen in the equivalent target plane images for (b) a single-frequency beam with an RPP, (c) a four-color beam with a 0.44-nm separation and RPP, and (d) a four-color beam with a 0.44-nm separation, 0.2 nm of FM bandwidth per color, and RPP. The normalized rms intensity variance, σ/I, for these images is (b) ~0.79, (c) ~0.25, and (d) ~0.16. (70-00-0395-0796pb01)

Theoretical modeling of the temporal dynamics of beam smoothing demonstrates that the multiple-aperture SSD technique described here can give very rapid and effective beam smoothing at the target plane. Simulations of the power spectra and the smoothing capability for (a) one-color SSD with 108 GHz of bandwidth at 1ω, (b) four colors with 136 GHz separation at 1ω and no FM bandwidth, and (c) four colors with 136 GHz separation and 54 GHz of bandwidth at 1ω are shown in Figs. 11 and 12. Figure 11(a) shows the spectrum for a one-color beam with 108 GHz of FM bandwidth at 1ω, 324 GHz at 3ω. There is sufficient dispersion to decorrelate each FM component of this spectrum at the target plane (0.21 μrad / GHz at 3ω). These values represent the maximum bandwidth / dispersion that can be propagated through the Nova chain with decorrelated spectral components without clipping in the spatial filter pinholes. The smoothing rate, $(d\sigma/dt)/\sigma$, reaches a peak rate of 0.11 ps^{-1} in 2–3 ps, comparable to the inverse of the total bandwidth. The intensity cross-correlation between the speckle field at

a given time and the initial speckle field drops from 1.0 to a value near zero in the same 2–3 ps. The normalized smoothing level, σ, drops from near unity to 0.707 in the first 2–3 ps, and to 0.5 in 8–10 ps, as shown in Fig. 12(a). It reaches an asymptotic level of ~0.15 after 1 ns, consistent with time-integrated smoothing levels previously measured on Nova under these conditions.[20]

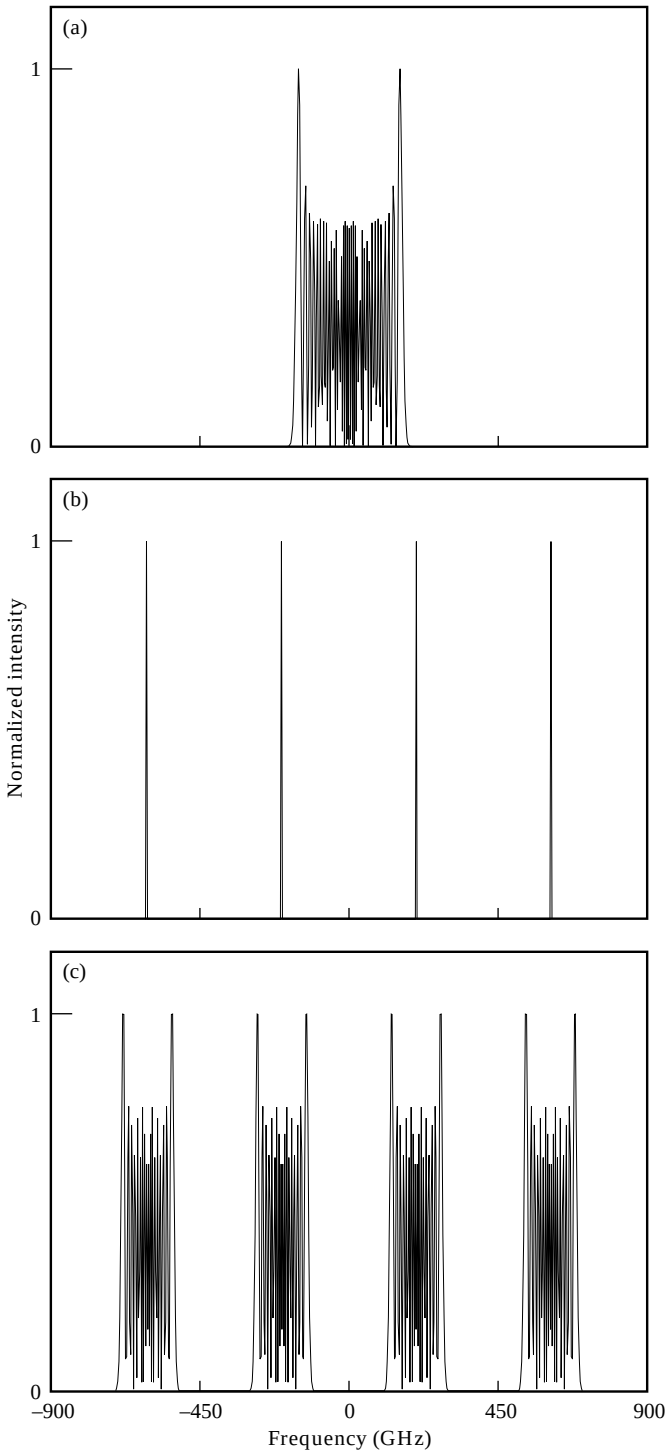

FIGURE 11. Power spectrum of a beam with (a) 324 GHz of FM bandwidth at 3ω, (b) four colors with 405 GHz separation at 3ω, and (c) four colors with 405 GHz separation and 162 GHz of FM bandwidth on each color. (70-00-0395-0797pb01)

Figure 11(b) shows the 3ω output spectrum for a four-color beam with frequencies separated by 136 GHz at 1ω or 405 GHz at 3ω. Figure 11(c) shows the same four-color spectrum, but with 54 GHz of 1ω FM bandwidth (162 GHz at 3ω) added to each of the four colors. We use a spectral dispersion of 0.29 μrad / GHz at 3ω in the simulations, corresponding to the value used in the four-color experiments on Nova. The initial smoothing rate for four-colors alone is five times faster than for the single-color FM bandwidth case. A peak rate of 5 ps^{-1} is achieved in less than 1 ps, corresponding to the inverse of the total frequency spread of 1.2 THz, reaching $\sigma = 0.5$ within 2.5 ps. The speckle field initially decorrelates in <1 ps, but the cross-correlation returns to unity at every beat period of the closest frequency spacing (405 GHz), and the field repeats every 2.47 ps. Thus even though the initial smoothing rate is very high, once σ reaches 0.5, as expected for the sum of four independent speckle fields, no further smoothing is obtained, as shown in Fig. 12(b). With the addition of FM bandwidth to each of the four colors, the initial high smoothing rate is still achieved, but the integrated smoothing level continues to decrease rapidly, reaching an asymptotic value of 0.08 in a few tens of picoseconds [Fig. 12(c)]. Since the overall spectrum is not continuous, the intensity cross-correlation shows secondary and tertiary peaks at times related to the beat frequencies of the principal four colors; however, these peaks are significantly damped within 8–10 ps, reducing in magnitude over one FM period when all frequency components are available for smoothing. The combination of four colors with FM bandwidth provides both a rapid initial smoothing level and effective time-averaged beam smoothing at the target plane.

3ω Four-Color Performance

To simulate the $f/8$ geometry proposed for the NIF, we retrofitted the four-color beamline to accommodate an $f/8$ target chamber lens on the 10-beam chamber. The incident beam diagnostic (IBD) is used to diagnose the 3ω performance of the four-color system.[33] The IBD records the spatially integrated 3ω energy, the near-field image, and the temporal pulse shape integrated over all four quadrants. Figure 13 shows a representative near-field image of the 3ω beam taken with the IBD CCD camera. The energy in the four quadrants is balanced to better than ±17%.

After installation on the 10-beam chamber, the four-color KDP array was rocked ±500 μrad to establish the best tuning coordinates, achieving a 3ω array efficiency

of up to 65%. This delivers up to 2.3 kJ at 3ω in 1 ns to the target. In addition, since the standard master oscillator is tuned 0.22 nm off Nd:YLF line center to produce the four-color beam, the pulse to the other nine arms is also shifted in frequency. Thus, the KDP arrays on the other nine arms of Nova are appropriately tuned to compensate for this shift. Conversion efficiencies on the other nine arms with the Nova Type II/Type II arrays at the shifted wavelength are within 10% of their nominal conversion efficiencies on YLF line center. The addition of 0.2 nm of FM bandwidth to the four-color beam and the other nine arms reduces the 3ω conversion efficiency by <5%.

Pointing experiments performed with the $f/8$ lens after the four-color array activation show the expected beam symmetry and size at best focus, with all four quadrants within 50 μm of their expected positions. The arrival of the four-color beam at target chamber center relative to the other nine arms is synchronized to within 20 ps using techniques developed for the Precision Nova project.[34] A 5.8-mm-diam, square element phase plate inserted in the four-color beamline after the $f/8$ lens, produces a 570-μm focal spot diameter with a peak intensity of 2×10^{15} W/cm^2 for target experiments. To determine the effectiveness of the four-color system in controlling instabilities in NIF-like plasmas, the Full-Aperture Backscatter Station was used to measure the spatial distribution of the backwards propagating SBS from a target in each of the four beam quadrants, as well as the wavelength-resolved temporal evolution of the SBS in each quadrant. Measurements show that the four-color system produces <1% SBS backscatter at >2×10^{15} W/cm^2 when used to

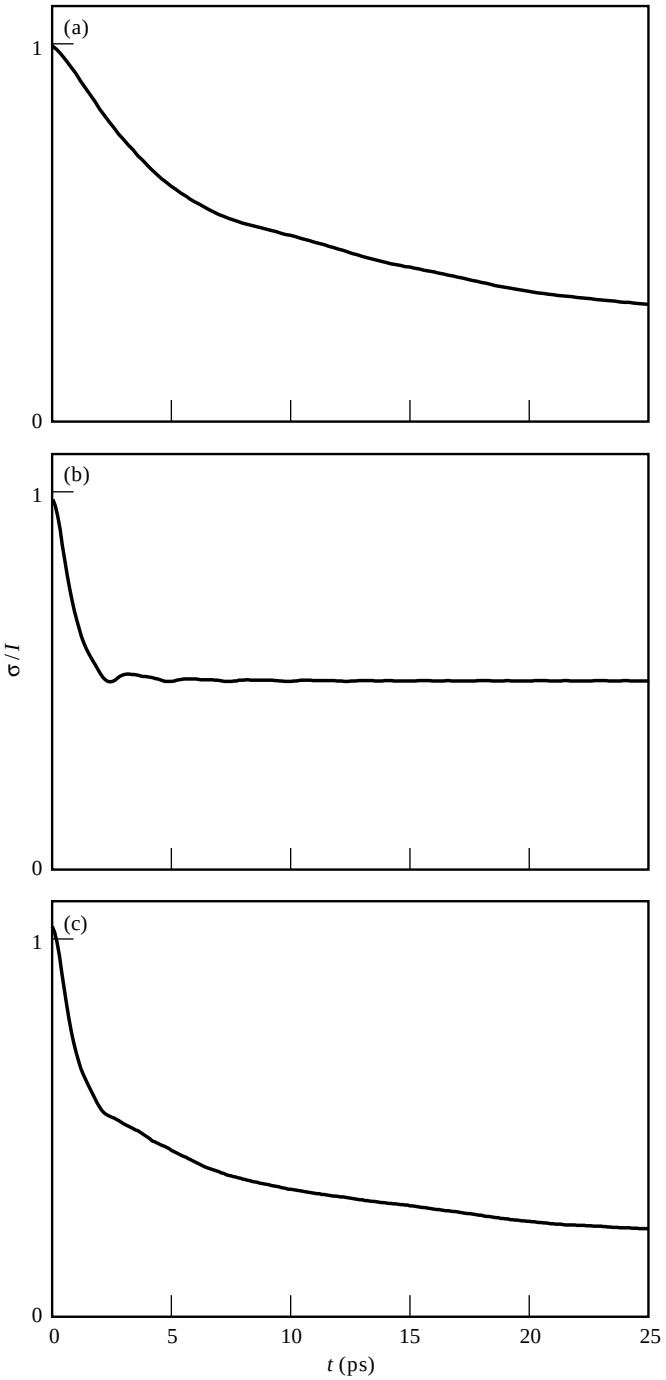

FIGURE 12. Calculated rms intensity variance, σ/I, of the focal irradiance plotted as a function of integration time for (a) 324 GHz of FM bandwidth at 3ω, (b) four colors with 405 GHz separation at 3ω, and (c) four colors with 405 GHz separation and 162 GHz of FM bandwidth on each color. (70-00-0395-0798pb01)

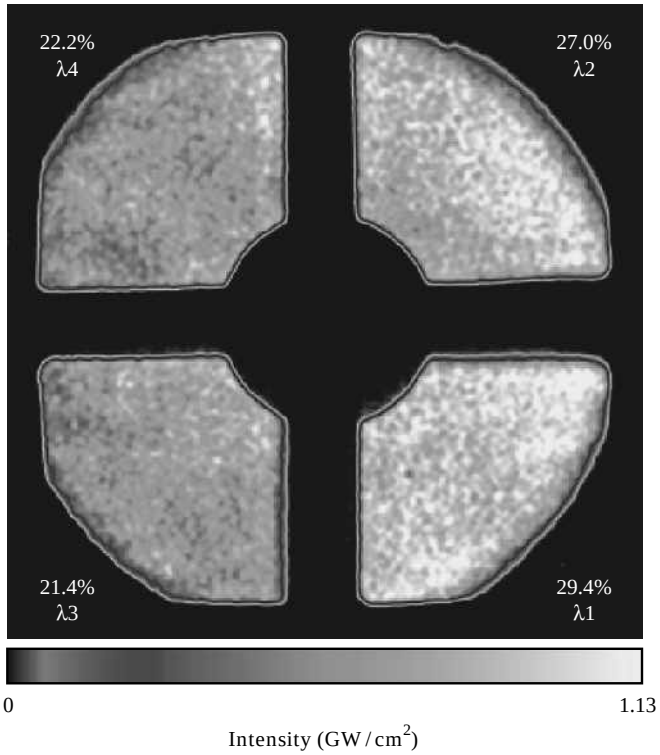

FIGURE 13. Representative near-field image of the 3ω beam taken with the incident beam diagnostic CCD camera in the 10-beam chamber area. The 3ω energy in each of the four quadrants balances to better than ± 17%. (70-00-0495-0924pb02)

probe NIF-like plasmas. Further details of the plasma physics experiments performed using the four-color system are described in "Laser–Plasma Interactions in Large Gas-Filled Hohlraums," p. 97 of this *Quarterly* and elsewhere. [13–15]

Summary

We successfully deployed a four-color bandwidth system with optical characteristics similar to that of the proposed NIF on Nova for laser experiments. A multifrequency bandwidth source is spatially separated into four quadrants, each containing a different central frequency, providing a total bandwidth of 1.32 nm at 1ω. The four colors are spatially separated into four quadrants using a novel grating multichrometer design. Each quadrant is independently converted to the third harmonic in a four-quadrant frequency conversion array with independent phase-matching, providing up to 2.3 TW at the third harmonic. The measured far-field irradiance shows ~25% rms intensity variation with four colors alone, reaching this level within 3 ps. The addition of 0.2 nm of FM bandwidth to each frequency component reduces the rms intensity variation level to ~16% without significant impact on the conversion efficiency.

Acknowledgments

The authors thank the Nova laser operators staff for their contributions and dedication, particularly E. Padilla, C. Brown, J. Vickers, and H. Orrell of the MOR, whose efforts throughout these experiments allowed us to achieve our goals. We also thank C. Brown and P. Danforth for their assistance with the development of the four-color bandwidth source. We gratefully acknowledge R. Ellis, R. Kent, and K. Stanion for mechanical design and activation of the four-color grating and frequency conversion arrays, and the $f/8$ lens assembly. We also thank our colleagues C. Laumann, J. Miller, R. Ehrlich, and C. Thompson for their contributions to the four-color diagnostics developed for these experiments, and S. Dixit for developing the phase plates.

Notes and References

1. S. Skupsky, et al., *J. Appl. Phys.* 66(8) 3456–3462 (1989).
2. H. T. Powell, S. N. Dixit, M. A. Henesian, *ICF Quarterly Report* 1(1), 28–38, Lawrence Livermore, National Laboratory, Livermore, CA, UCRL-LR-105821-91-1 (1991).
3. P. H. Chaffee, F. G. Patterson, M. A. Henesian, *Technical Digest, Conference on Lasers and Electro-Optics* 10 (Optical Society of America, Anaheim, CA, 1989) p. 106.
4. M. A. Henesian, et al., *Technical Digest, International Quantum Electronics Conference* 9, Paper TuE3 (1992).
5. S. P. Obenschain, et al., *Phys. Rev. Lett.* 56, 2807 (1986).
6. W. L. Kruer, *The Physics of Laser Plasma Interactions* (Addison–Wesley,NY, 1988).
7. J. F. Drake, et al., *Phys. Fluids* 17(9), 778 (1974).
8. R. L. Berger, *Phys. Rev. Lett.* 65, 1207–1210 (1990).
9. W. Seka, et al., *Phys. Fluids B* 4, 2232–2240 (1992).
10. R. L. McCrory, et al., *Laser Part. Beams* 8, 27–32 (1990).
11. J. A. Paisner, *National Ignition Facility Conceptual Design Report*, Lawrence Livermore National Laboratory, Livermore, CA, UCRL-PROP-117093 (1994).
12. D. M. Pennington, et al., *Technical Digest, Conference on Lasers and Electro-Optics* 8 (Optical Society of America, Anaheim, CA, 1994) p. 161.
13. L. V. Powers, et al., *Phys. Rev. Lett.* 74, 2957–2960 (1995).
14. B. J. MacGowan, et al., "The Study of Parametric Instabilities in Large-Scale-Length Plasmas Produced by Laser Irradiation of Thin-Walled Gas-Balloons," Lawrence Livermore National Laboratory, Livermore, CA, UCRL-JC-117044 ABS; prepared for *Anomalous Absorption Conference*, Pacific Grove, CA, June 5–10, 1994, p. AO–1.
15. D. S. Montgomery, et al., "Experimental Study of SBS and SRS in the Nova Gas-Target Large Plasmas," Lawrence Livermore National Laboratory, Livermore, CA, UCRL-JC-117072 ABS; prepared for *Anomalous Absorption Conference*, Pacific Grove, CA, June 5–10, 1994, p. BP–22.
16. Y. Kato, et al., *Phys. Rev. Lett.* 53(11), 1057–1060 (1984).
17. S. N. Dixit, et al., *Appl. Opt.* 32, 2543–2554 (1991).
18. L. V. Powers, et al., "Gas-Filled Targets for Large Scalelength Plasma Interaction Experiments on Nova," Lawrence Livermore National Laboratory, Livermore, CA, UCRL-JC-118104(1995); to be published in *Physics of Plasmas*.
19. B. F. Lasinski, et al., "SBS and Filamentation in Current and Future Experiments," Lawrence Livermore National Laboratory, Livermore, CA, UCRL-JC-116795 ABS, Rev 1; prepared for *Anomalous Absorption Conference*, Pacific Grove, CA, June 5–10, 1994, p. AP–14.
20. D. M. Pennington, et al., *Proc. Soc. Photo–Instrum. Eng.* 1870, 175–185 (1993).
21. R. H. Stolen, C. Lin, *Phys. Rev. A* 17, 1448–1453 (1978).
22. J. R. Thompson and R. Roy, *Phys. Rev. A* 43, 4987–4996 (1991).
23. D. J. Kuizenga, *Laser Program Annual Report–79*, Lawrence Livermore National Laboratory, Livermore, CA, UCRL-50021-79 (1980).
24. R. B. Wilcox, *Lasers Part. Beams* 4, 141–143 (1986).
25. J. K. Lawson, et al., *Appl. Opt.* 31, 5061–5068 (1992).
26. R. D. Boyd, et al., *Appl. Opt.* 34, 1697–1706 (1995).
27. P. J. Wegner, et al., *Appl. Opt.* 31, 6414–6426 (1992).
28. S. E. Stokowski, R. A. Saroyan, M. J. Weber, *Laser Glass Handbook*, Lawrence Livermore National Laboratory, Livermore, CA, M-095, Rev. 2 (1981).
29. P. J. Wegner, M. A. Henesian, *Proc. Soc. Photo–Opt. Instrum. Eng.* 1414, 162 (1991).
30. T. Jitsuno and N. Nishi, Osaka University, ILE, Osaka, Japan, private communication (May 16, 1994).
31. M. A. Henesian, C. D. Swift, J. R. Murray, *Opt. Lett.* 10, 472 (1985).
32. M. D. Skeldon, et al., IEEE J. *Quantum Electron.* 28, 1389–1399 (1992).
33. C. W. Laumann, et al., *ICF Quarterly Report* 4(1), 1–9, Lawrence Livermore National Laboratory, Livermore, CA, UCRL-LR-105821-94-1 (1993).
34. J. A. Caird, et al., *ICF Quarterly Report* 4(1), 10–17, Lawrence Livermore National Laboratory, Livermore, CA, UCRL-LR-105821-94-1 (1993).